Lecture 10. Surface Energy Balance (Garratt 5.1-5.2)

In this lecture…

- Diurnal cycle of surface energy flux components over different surfaces
- Radiative and material properties of different surfaces
- Conductive penetration of surface temperature variations into the ground.

The balance of energy at the earth's surface is inextricably linked to the overlying atmospheric boundary layer. In this lecture, we consider the energy budget of different kinds of surfaces. Consider first an ideal surface, which is a very thin interface between the air and an underlying solid or liquid medium that is opaque to radiation. Because it is thin, this surface has negligible heat capacity, and conservation of energy at the surface requires that

$$R_N = H_S + H_L + H_G, \tag{10.1}$$

where (note sign conventions):

H_S (often just called H) is the upward surface sensible heat flux

$H_L = LE$ is the upward surface latent heat flux due to evaporation at rate E

H_G is the downward **ground heat flux** into the subsurface medium.

R_N is the net downward radiative flux (longwave + shortwave).

$L = 2.5\times10^6$ J kg^{-1} is the latent heat of vaporization. The **Bowen ratio** $B = H_S / H_L$.

Over land, there is a large diurnal variation in the surface energy budget (see Figure 10.1). Over large bodies of water, the large heat capacity of the medium and the absorption of solar radiation over a large depth combine to reduce the near-surface diurnal temperature variability, so H_S and H_L vary much less. However, the surface `skin temperature' of a tropical ocean can vary diurnally by up to 3 K in sunny, light-wind conditions.

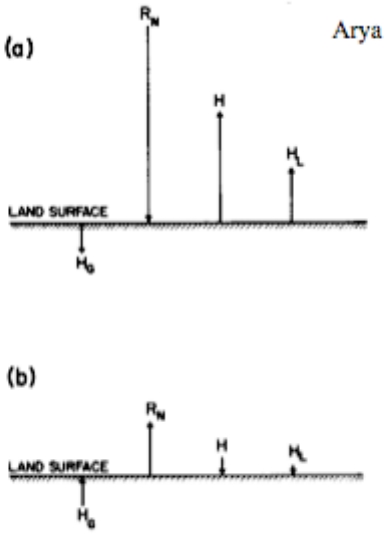

Fig. 2.1 Schematic representation of typical surface energy budgets during (a) daytime and (b) nighttime.

Fig. 10.1

Arya

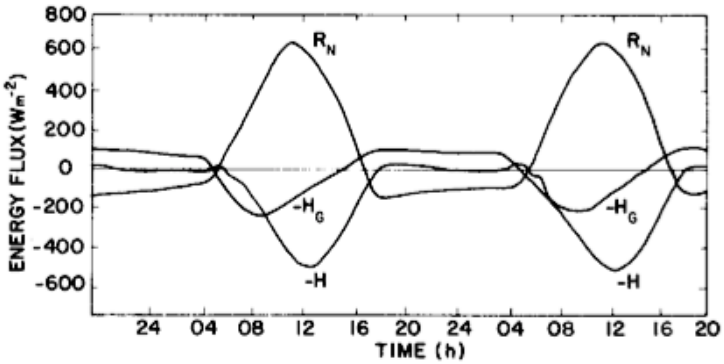

Fig. 2.3 Observed diurnal energy balance over a dry lake bed at El Mirage, California, on June 10 and 11, 1950. [After Vehrencamp (1953).]

Fig. 10.2

An ideal surface is not usually encountered. Real surfaces may include a plant canopy or other features such as buildings not opaque to radiation and with a significant heat capacity. In this case, it is more appropriate to define an interfacial layer which includes such features. We let $W(t)$ be the energy stored within this layer per unit horizontal area. The revised layer energy budget is:

$$R_N = H_S + H_L + H_G + dW/dt. \tag{10.2}$$

We could also consider the energy budget of control volumes with finite horizontal extent (e. g. a parking lot, city, or larger geographic region). In this case horizontal transfer of energy may also be important; we won't consider this complication here.

Examples

The energy budget measured over a dry desert lake bed is shown in Fig. 10.2. In this case, latent heat fluxes are negligible. During the day, copious solar radiation is absorbed at the surface, and the ground heats up rapidly. Initially, most of the heat is conducted down into the soil, but as the layer of warmed soil thickens, H_S dominates; the heat is primarily transferred to the air. This is promoted by extreme differences (up to 28 K) between the ground temperature and the 2 m air temperature. At night, surface radiative cooling is balanced by an upward ground heat flux. Since the nocturnal boundary layer is very stable, the turbulent heat flux H_S is negligible.

The energy budget of a barley field is shown in Fig. 10.3. During the daytime, radiative heating of the surface is balanced mainly by latent heat flux due to evapotranspiration, i. e. evaporation from the soil surface and transpiration by the plant leaves. In the lingo, the Bowen ratio is small,

Arya

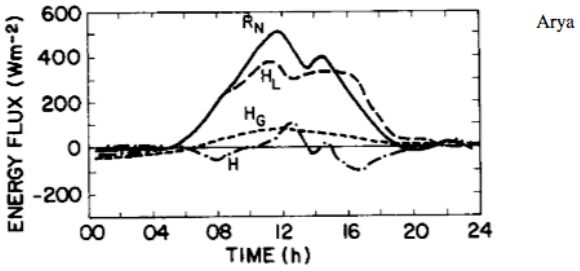

Fig. 2.4 Observed diurnal energy budget of a barley field at Rothamsted, England, on July 23, 1963. [From Oke (1987); after Long *et al.* (1964).]

Fig. 10.3

Arya

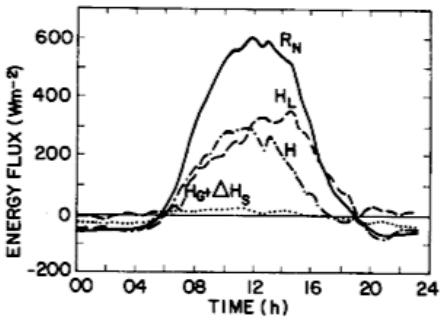

Fig. 2.5 Observed energy budget of a Douglas fir canopy at Haney, British Columbia, on July 23, 1970. [From Oke (1987); after McNaughton and Black (1973).]

Fig. 10.4

-0.3 to 0.3. H_L can be so large that the surface gets cooler than the air during early morning and late afternoon and the heat flux is downward. For a field, heat storage is usually negligible. At night, all terms become much smaller; as before, radiative cooling is mainly balanced by ground heat flux.

The last example is a Douglas fir forest (Fig. 10.4). Here latent and sensible heat fluxes are comparable during the day. The storage and ground heat flux are lumped in the curves, but for deep forest, the storage term dominates. At night, release of heat from the tree canopy and condensation (dew) balance radiative energy loss.

Net radiation at the surface

The net radiation R_N is due to the difference between downwelling and upwelling shortwave plus longwave radiative fluxes. The net shortwave flux depends on the incident solar radiation $R_{S\downarrow}$ and on surface albedo a_s. The net longwave flux depends upon the downwelling longwave radiation $R_{L\downarrow}$, the surface emissivity ε_s, and the radiating temperature T_s:

$$R_N = R_{S\downarrow} - R_{S\uparrow} + R_{L\downarrow} - R_{L\uparrow} = (1 - a_s)R_{S\downarrow} + R_{L\downarrow} - \{(1- \varepsilon_s)R_{L\downarrow} + \varepsilon_s\sigma_s T_s^4\}$$
$$= (1 - a_s)R_{S\downarrow} + \varepsilon_s (R_{L\downarrow} - \sigma_s T_s^4\}. \qquad (10.3)$$

Thus, the surface characteristics critically influence R_N. Table 10.1 gives typical surface radiative characteristics. Albedos are quite diverse, while emissivities are usually near, but not equal, to 1.

Arya

Table 3.1
Radiative Properties of Natural Surfaces[a]

Surface type	Other specifications	Albedo (a)	Emissivity (ε)
Water	Small zenith angle	0.03–0.10	0.92–0.97
	Large zenith angle	0.10–0.50	0.92–0.97
Snow	Old	0.40–0.70	0.82–0.89
	Fresh	0.45–0.95	0.90–0.99
Ice	Sea	0.30–0.40	0.92–0.97
	Glacier	0.20–0.40	
Bare sand	Dry	0.35–0.45	0.84–0.90
	Wet	0.20–0.30	0.91–0.95
Bare soil	Dry clay	0.20–0.35	0.95
	Moist clay	0.10–0.20	0.97
	Wet fallow field	0.05–0.07	
Paved	Concrete	0.17–0.27	0.71–0.88
	Black gravel road	0.05–0.10	0.88–0.95
Grass	Long (1 m)	0.16–0.26	0.90–0.95
	Short (0.02 m)		
Agricultural	Wheat, rice, etc.	0.10–0.25	0.90–0.99
	Orchards	0.15–0.20	0.90–0.95
Forests	Deciduous	0.10–0.20	0.97–0.98
	Coniferous	0.05–0.15	0.97–0.99

[a] Compiled from Sellers (1965), Kondratyev (1969), and Oke (1978).

Table 10.1

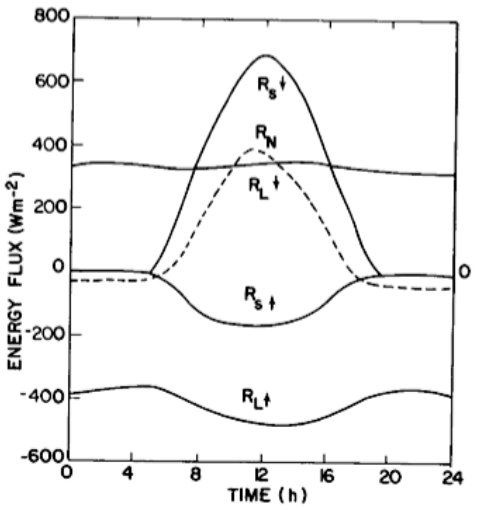

Fig. 3.4 Observed radiation budget over a 0.2-m-tall stand of native grass at Matador Saskatchewan, on July 30, 1971. [From Oke (1987); after Ripley and Redmann (1976).]

Fig. 10.5

An example of the surface radiation components is shown in Fig. 10.5.

Soil temperatures and heat flux

The surface or skin temperature is important for the radiative balance of the surface and for predicting frost and dew. It can be quite different than the `surface' air temperature, which is conventionally measured at 1.5-2 m. In fact, it can be difficult to even measure in situ because it is difficult to shield and ventilate a sensor placed at the surface. Furthermore, if there is a plant canopy or surface inhomogeneity, there is no single uniquely definable surface temperature. Radiatively, an apparent surface temperature can be determined from the upward longwave energy flux if the emissivity is known. Large diurnal variations in skin temperature are achieved for bare, dry surfaces in clear calm conditions. Under such conditions, midday skin temperature may reach 50-60 C, while early morning skin temperatures can drop to 10-20 C.

The surface temperature is related to the temperature profile in the subsurface medium, as illustrated in Figs 10.6-7. In a solid medium, the subsurface temperature profile is governed by heat conduction. Deeper in the soil, the diurnal temperature cycle decreases and lags the cycle of skin temperature. Over an annual cycle, similar waves penetrate further into the soil.

If z is depth into the soil and $T(z, t)$ is soil temperature, Fourier's law of heat conduction states:

$$H_G = -\kappa \partial T/\partial z, \quad (\kappa = \text{thermal conductivity})$$

Thermal energy conservation implies that

$$\rho c \frac{\partial T}{\partial t} = -\frac{\partial H_G}{\partial z} \quad (\rho = \text{density}, c = \text{heat capacity})$$

Combining these two equations and assuming that the subsurface medium is homogeneous, so that material constants do not depend on z, we obtain the diffusion equation

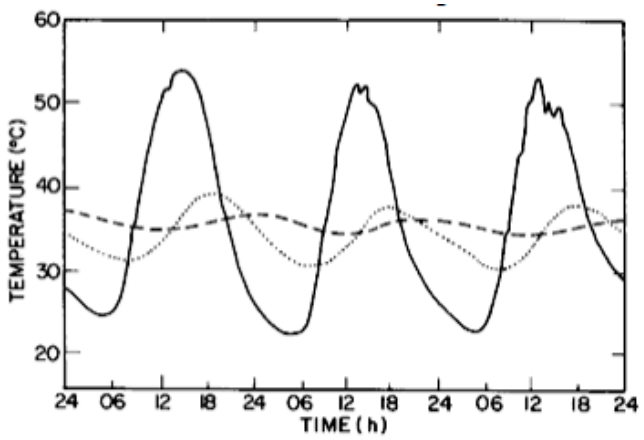

Fig. 4.1 Observed diurnal course of subsurface soil temperatures at various depths in a sandy loam with bare surface. ——, 2.5 cm; ·····, 15 cm; ---, 30 cm. [From Deacon (1969); after West (1952).]

Fig. 10.6

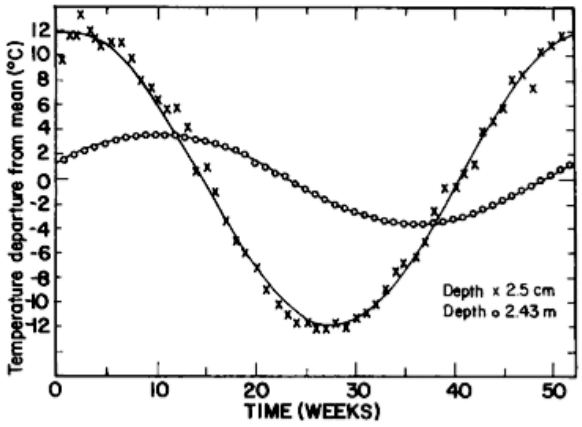

Fig. 4.2 Annual temperature waves in the weekly averaged subsurface soil temperatures at two depths in a sandy loam soil. ×, 2.5 cm; ○, 2.43 m. Fitted solid curves are sine waves. [From Deacon (1969); after West (1952).]

Fig. 10.7

$$\frac{\partial T}{\partial t} = \kappa \frac{\partial^2 T}{\partial z^2} \qquad (\kappa = k/\rho c = \text{thermal diffusivity}) \tag{10.4}$$

Table A7 from Garratt (next page) gives properties of various materials; the thermal conductivity varies over almost two orders of magnitude from new snow (low) to rock (high). Wet soils have conductivities about five times as large as dry soils. The thermal diffusivity shows similar trends, but less variation. Surprisingly, κ is smallest for water due to its large heat capacity.

It is illuminating to look at a soil temperature wave forced by a sinusoidal variation in surface temperature. We assume a deep soil temperature $T(z \to \infty) = \overline{T}$ and take $T(0) = \overline{T} + A \cos \omega t$. We look for a solution to (10.4) that is also sinusoidal in time with the same frequency ω:

Table A7. *Representative values of the thermal conductivity k_s, specific heat c_s, density ρ_s and thermal diffusivity κ_s for various types of surface based mainly on Table* 11-3 *in Pielke* (1984) Garratt

Data for clay and sand are approximately consistent with Eq. A24, in which C_{si} is equal to 2.7×10^6 and 2.2×10^6 J m^{-3} K^{-1} for clay and sand respectively; C_w is equal to $\rho_w c_l$, with $\rho_w = 1000$ kg m^{-3} and $c_l = 4186$ J kg^{-1} K^{-1}; and η_s is taken from Table A9. The reader should also consult e.g. Geiger (1965, Table 10), Hillel (1982, Table 9.3) and Oke (1987, Table 2.1).

Surface	k_s (W m^{-1} K^{-1})	c_s (J kg^{-1} K^{-1})	ρ_s (kg m^{-3})	κ_s (10^{-6} m^2 s^{-1})
Sand soil				
dry	0.3	800	1600	0.23
$\eta = 0.2$	1.9	1260	1800	0.84
$\eta = 0.4$	2.2	1480	2000	0.74
Clay soil				
dry	0.25	890	1600	0.18
$\eta = 0.2$	1.1	1170	1800	0.52
$\eta = 0.4$	1.6	1550	2000	0.52
rock	2.9	750	2700	1.4
ice	2.5	2100	910	1.3
snow				
old	1.0	2090	640	0.7
new	0.1	2090	150	0.3
water	0.6	4186	1000	0.14

$$T(z,t) = \overline{T} + \mathrm{Re}\{a(z)\exp(i\omega t)\}$$

Here $a(z)$ is a complex-valued function of z. To satisfy (1):

$$i\omega a = -\kappa \, d^2a/dz^2 \qquad (10.5)$$

To satisfy the boundary conditions,

$$a(0) = A, \; a(z \to \infty) = 0$$

The solution of (10.5) that satisfies the BCs is

$$a(z) = A \exp(-[1 + i]z/D), \; D = (2\kappa/\omega)^{1/2}$$

$$T(z,t) = \mathrm{T} + \exp(-z/D)\cos(\omega t - z/D) \qquad (10.6)$$

This solution is shown in Fig. 10.8. The temperature wave damps exponentially with depth z, and lags the surface temperature wave by a phase z/D, which increases with depth. Fig. 10.9

provides beautiful observational confirmation of this prediction. The **damping depth** D to which the temperature wave penetrates increases as the oscillation frequency slows and is larger if the thermal diffusivity is larger. For moist soil ($\kappa = 0.8\times10^{-6}$ m^2s^{-1}), $D = 0.14$ m for the diurnal cycle and 2.8 m for the annual cycle.

The ground heat flux at the surface is

$$H_G = -k\,\partial T/\partial z = -\rho c \kappa A/D\ \mathrm{Re}\{[1+i]\exp(i\omega t)\} = \rho c(\kappa\omega)^{1/2} A\cos(\omega t + \pi/4)$$

It leads the surface temperature wave by 1/8 cycle. Hence, the ground heat flux is largest three hours ahead of the surface temperature for a diurnally varying surface temperature cycle.

In practice, the diurnal cycle of surface temperature is not sinusoidal. Furthermore, the surface temperature interacts with the sensible and latent heat fluxes so that the surface boundary condition is really the energy balance of the surface, which is coupled to the atmosphere. Lastly, testing of these formulas is complicated by the fact the temperature within 1 cm of the ground can be nonuniform, so the surface temperature and ground heat flux must be inferred from measurements across a buried `flux plate', a thin plate buried within the soil that measures heat flux based on the temperature difference across it, typically at a depth of 1-2 cm.

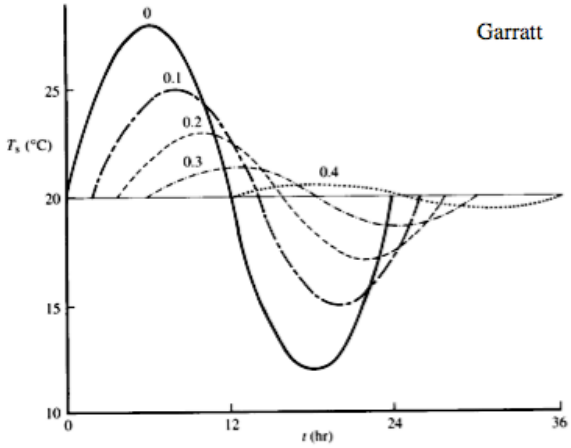

Fig. 5.1 Idealized variation of soil temperature through a diurnal cycle for several depths in the soil (indicated in metres). The curves represent the solutions to Eq. 5.7 for sinusoidal forcing; these are given by Eq. 5.8. A uniform soil is assumed with $\kappa_s = 0.8 \times 10^{-6}\ m^2\,s^{-1}$ and $k_s = 1.68\ W\,m^{-1}\,K^{-1}$.

Fig. 10.8

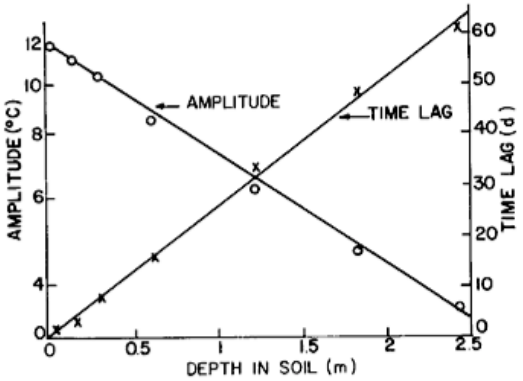

Fig. 4.4 Variations of amplitude and time lag of the annual soil temperature waves with depth in the soil. [From Deacon (1969).]

Fig. 10.9